



# High performance supercapacitor behavior of hydrothermally synthesized CdTe nanorods

M. Manikandan<sup>1</sup> · P. Nisha Francis<sup>1</sup> · S. Dhanuskodi<sup>1</sup> · N. Maheswari<sup>2</sup> · G. Muralidharan<sup>2</sup>

Received: 10 May 2018 / Accepted: 6 August 2018 / Published online: 1 September 2018  
© Springer Science+Business Media, LLC, part of Springer Nature 2018

## Abstract

CdTe nanorods (NRs) have been prepared by hydrothermal process using ascorbic acid as a reducing agent. X-ray diffraction pattern reveals the formation of CdTe with cubic structure. From transmission electron microscopy the morphology of CdTe is found to be NRs with the length and diameter of 176 and 43 nm respectively. Brunauer–Emmett–Telle and Barrett–Joyner–Halenda analyses show the surface area ( $12.16 \text{ m}^2/\text{g}$ ), pore volume ( $0.13 \text{ cm}^3/\text{g}$ ) and pore diameter (44 nm). A high specific capacitance (438 F/g) is obtained at the current density of  $2 \text{ mA}/\text{cm}^2$  by the galvanostatic charge–discharge method. The excellent cyclic stability (95%) and the Coloumbic efficiency (99.7%) have been achieved even after 5000 cycles. The symmetric supercapacitor device exhibits the specific capacitance of 103 F/g at current density of  $2.5 \text{ mA}/\text{cm}^2$  with an energy density of 20.54 Wh/kg. The high density and electrochemical stability of the prepared CdTe electrode is a promising material for electrochemical energy storage devices.

## 1 Introduction

Recently, a considerable attention has been paid to the synthesis of micro and nano structured materials due to their interesting properties and exciting functionalities. One dimensional nanostructure including nanowires, nanotubes, nanofibers and nanorods (NRs) has attracted a great amount of interest with their unique assets derived from the dimensionality dependent anisotropy. Especially, metal tellurides like ZnTe, CdTe, LaTe, NiTe have been extensively investigated because of their applications in photonics and bioimaging devices namely light emitting diodes (LEDs), solar cells, supercapacitors and biosensors [1]. PbSe/rGO nanocomposite displays a high current density compared with PbSe nanocubes due to high responsivity ( $14 \text{ mA}/\text{W}$ ) and detectivity ( $1.6 \times 10^8 \text{ Jones}$ ) [2]. Yousefi et al. have studied the photocatalytic activity for ZnSe quantum dots (QDs) and ZnSe/rGO nanocomposite for methylene blue dye. Orange emission plays an important role in the enhancement of the photocatalytic degradation (66%) of ZnSe/rGO

QDs nanocomposite [3]. Nanowires of ZnTe and PbTe have been fabricated by the chemical vapour deposition method and the photocurrent ( $4.8$  and  $3.59 \text{ mA}/\text{cm}^2$ ) and photovoltaic efficiency  $\eta$  (0.65 and 1.11%) are determined [4]. The concentration of rGO greatly enhances the photocatalytic degradation of SnSe nanostructures against methylene blue dye (69%) and phenol (50%) [5].

Electrochemical capacitors also known as supercapacitors/ultracapacitors have drawn much attention as a new kind of energy storage device by its high efficiency, high power density, fast charge/discharge, environmental friendliness and longer cycling life span over the conventional batteries [6, 7]. Based on the charge storage mechanism, they can be classified as electrochemical double layer capacitor (EDLC) and pseudocapacitor. Carbon based compounds store the energy in the form of EDLC while metal oxides, metal chalcogenides and conducting polymers belong to the class of pseudocapacitor in which the storage is via fast Faradic reactions [8, 9]. Transition metal chalcogenides (TMC) find various electrochemical applications such as sensors, batteries, catalysts and supercapacitor due to their high surface area, high electrical conductivity [10, 11]. TMC materials are promising cathodes for lithium and sodium ion batteries due to their high density, small volume, long life time, low cost and eco-friendliness. Chao et al. have synthesized Li/LiPF<sub>6</sub>/Cu<sub>x</sub>Te cell for Li ion batteries. It exhibits the highest specific

✉ S. Dhanuskodi  
dhanus2k3@yahoo.com

<sup>1</sup> School of Physics, Bharathidasan University,  
Tiruchirappalli 620 024, India

<sup>2</sup> Department of Physics, Gandhigram Rural Institute –  
Deemed University, Dindigul 624 302, India

capacity (280 mA/hg) and high cyclic stability (even after 5000 cycles) [12]. In order to increase the device performance and efficiency, now the researchers are focusing on TMCs such as  $\text{Sm}_2\text{Te}_3$  [8],  $\text{Sm}_2\text{S}_3$  [9],  $\text{NiS}_2$  [13],  $\text{Te}$  [14],  $\text{La}_2\text{Te}_3$  [15] etc. as electrode materials because of their low cost, easiness to fabricate and large capacitance.

Cadmium telluride (CdTe) is a II–VI semiconductor with a direct band gap of 1.47 eV at room temperature. Its high absorption coefficient in the visible region makes it a suitable material for photovoltaics. Also, its band gap can be tuned by doping Zn or Hg in the Cd site to open up new opportunities in the field of X-ray,  $\gamma$ -ray and infrared detectors [16]. Though CdTe in bulk single crystal shows zinc blende structure, it can also exist in the hexagonal, wurtzite form like other II–VI semiconductors (CdS, CdSe) [17, 18]. Many approaches like hydrothermal [1], electrodeposition [16], thinfilm [19] and solvothermal [20] have been deployed to synthesize nanocrystalline CdTe with various morphologies. CdTe nanoribbons were synthesized for the first time via a two-step process to be used as visible-NIR photodetectors [21]. Cathodically electrodeposited with controlled composition of CdTe NRs were prepared to study the current–voltage characteristics. This indicates the presence of Schottky barriers at both ends of Au/CdTe interface and under optical illumination, single CdTe NWs exhibits enhanced conductance [6]. Photoresponse device fabricated using CdTe NRs exhibit high photocurrent decay ratio (99.99%), high responsivity ( $\approx 6.90$  A/W), fast response time and no decay tail under 632.8 nm He–Ne laser illuminations. These High-quality straight and multiply kinked CdTe nanowires open up potential applications in the bottom-up integrated nanoelectronic and nanophotonic systems such as photovoltaic and multi terminal nanodevices [17]. Cd is present in photovoltaics modules and C-size flashlight battery. NiCd battery can be recharged 700–1200 times over its life in a per kWh basis. It has a high specific energy, energy density, life cycle, fast charging, recyclability, low cost and efficiency compared with some other Ni batteries [22, 23]. Eventhough the synthesis of CdTe NRs are well investigated, most of the reports deal with the structural properties and the optical characterizations. Attracted by the excellent properties and potential applications of CdTe NRs, an attempt is made to understand its electrochemical behavior and their

role in energy storage devices. In, this work, CdTe NRs for supercapacitor application has been studied in this work.

## 2 Materials and methods

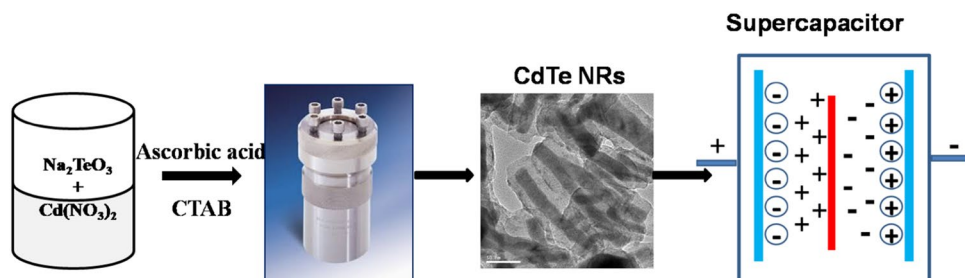
### 2.1 Synthesis of CdTe NRs

Cetyltrimethylammonium bromide (CTAB), sodium telluride ( $\text{Na}_2\text{TeO}_3$ ) (Sigma Aldrich) and ascorbic acid ( $\text{C}_6\text{H}_8\text{O}_6$ ), cadmium nitrate tetrahydrate  $\text{Cd}(\text{NO}_3)_2 \cdot 4\text{H}_2\text{O}$  (Merck) were used as the starting materials. Deionized water from a Milli-Q ultrapure (18.2 M $\Omega$ /cm) was used. CdTe NRs were synthesized by hydrothermal method [24]. 14.2 mmol of  $\text{C}_6\text{H}_8\text{O}_6$  was dissolved in 40 ml of deionized water under mild magnetic stirring at room temperature followed by the addition of 0.82 mmol of CTAB. In the next step, when 1.88 mmol of  $\text{Na}_2\text{TeO}_3$  and 1.88 mmol of  $\text{Cd}(\text{NO}_3)_2 \cdot 4\text{H}_2\text{O}$  were added to the solution,  $\text{TeO}_2$  was precipitated (white) immediately. Finally, 40 ml of deionized water was added and the final solution was transferred into a 100 ml Teflon-lined stainless steel autoclave, sealed and maintained at 180 °C for 24 h in an oven which was then allowed to cool to room temperature. The obtained black powder was collected and washed with deionized water and ethanol several times and dried at 60 °C for 12 h. A schematic diagram for the synthesis and characterization of CdTe NRs is given in Fig. 1.

### 2.2 Material characterization

X-ray diffraction (XRD) was carried out (PANalytical X-pert pro) with  $\text{CuK}\alpha$  (1.5406 Å) in the  $2\theta$  range from 10° to 80°. Micro Raman spectrum (Witec Confocal CDM 200) was recorded with 488 nm laser excitation. Morphological analysis was performed with FESEM (Hitachi High Tech SU 6600) and transmission electron microscopy (TEM) (FEI-Tecna microscope equipped with a LaB6 filament at an operating voltage of 200 kV).  $\text{N}_2$  adsorption–desorption isotherms at 77 K experiment was carried out using micromeritic ASAP 3020 analyzer and the surface area and pore size were determined by Brunauer–Emmett–Teller (BET) analyzer.

**Fig. 1** Schematic representation for the synthesis of CdTe NRs for supercapacitor applications



## 2.3 Fabrication of the three electrode supercapacitor

CdTe (1 mg), activated carbon and polytetrafluoro ethylene were mixed (80:15:5) with the addition of ethanol. The slurry was coated on to a graphite sheet of area 1 cm<sup>2</sup>. The electrochemical experiment (CHI 660D electrochemical workstation) was carried out using a single compartment three electrode system with CdTe as the working electrode, platinum as the counter electrode and Ag/AgCl as the reference electrode with 2 M of KOH as the electrolyte. The charge and discharge characterization was performed at current density from 2 to 30 mA/cm<sup>2</sup> within a potential window of –1.0 to 0.2 V.

## 2.4 Fabrication of symmetric supercapacitor

Symmetric type of supercapacitor was assembled using CdTe NRs as electrode material and non-woven as separator and 2 M of KOH as electrolyte. CV and GCD measurement for symmetric supercapacitor were performed using CHI 660D electrochemical workstation. The charge and discharge characterization was performed at current density from 2.5 to 20 mA/cm<sup>2</sup> within a potential window of 0–1.2 V.

## 3 Results and discussion

### 3.1 Structural and morphological

Figure 2a shows the XRD pattern of CdTe NRs. With the presence of (111), (200), (220), (311), (331), (422) and (511) planes, the cubic structure of CdTe (JCPDS No. 65-0880, lattice parameter  $a = 6.477 \text{ \AA}$ ) is confirmed. The well distinguished and crystalline peaks with no other impurity peaks indicate the formation of single phase of CdTe. The Raman spectrum shown in Fig. 2b reveals the presence of carbon

with CdTe NWs. Two peaks at 1327 and 1581 cm<sup>-1</sup> are attributed to the D (to double resonance effect) and G bands (in plane vibration of graphitic carbon) in carbonaceous solid.

FESEM image of CdTe NRs is shown in Fig. 3a. Yong et al. [24] have reported different CdTe nanostructures, morphology varying with reaction time by the hydrothermal method. Figure 3b shows the TEM image of CdTe NRs. It is found that the outer region of NRs is uniformly coated with amorphous sheaths. Therefore, from the TEM micrograph, it is concluded that the existence of amorphous sheaths on the outer surface of the NRs is due to the presence of carbon. The length and diameter of the NRs are 200, 46 nm (with) and 176, 23 nm (without carbon sheath) respectively and the aspect ratio of NRs is 4.3. Figure 3c depicts the lattice resolved TEM image of CdTe NRs with the interplanar spacing of 0.488 nm corresponding to the (111) plane of cubic CdTe. The SAED pattern in Fig. 3d shows a well defined diffraction spots indicating the polycrystalline structure of the CdTe NRs. During the synthesis due to the carbonization of the ascorbic acid, carbon shells are formed over the surface of the Te NRs. Then Cd<sup>2+</sup> ions diffuse through the carbon shells and react with Te NRs to form CdTe NRs [24]. EDAX confirms the presence of C, Cd, Te and O (Fig. 3e). Te is easily oxidized in the air atmosphere therefore there is a possibility for the formation of Te (IV).

### 3.2 BET analysis

Nitrogen adsorption and desorption isotherms were obtained in order to determine the surface area and porosity of CdTe NRs. The product exhibits a type IV adsorption/desorption isotherms with a H3 type of hysteresis loop which is characterized for mesoporous materials and often associated with a narrow slit shaped (Fig. 4a). BET surface area of CdTe NRs is 12.16 m<sup>2</sup>/g with a pore volume of 0.13 cm<sup>3</sup>/g. The Barrett–Joyner–Halenda (BJH) average pore diameter is 44 nm

**Fig. 2** a XRD pattern and b micro-Raman spectrum of CdTe NWs

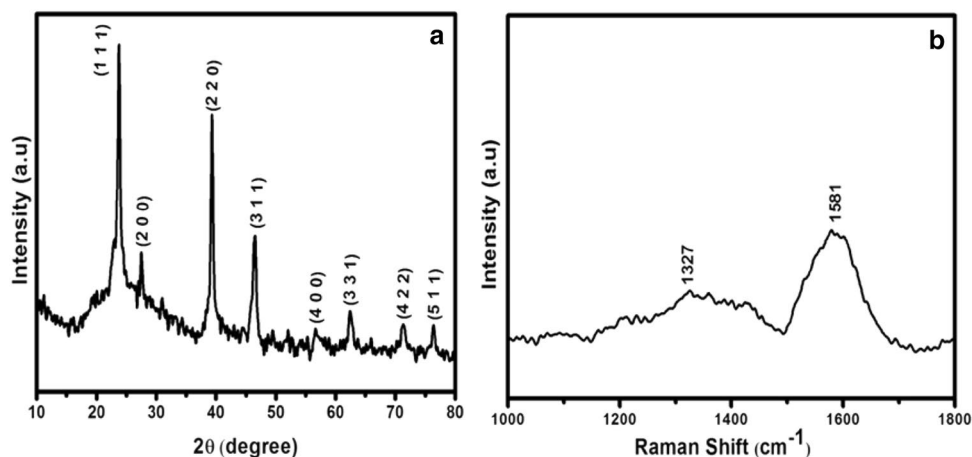


**Fig. 3** **a** FESEM, **b** TEM, **c** HRTEM, **d** SAED and **e** EDAX of CdTe NRs

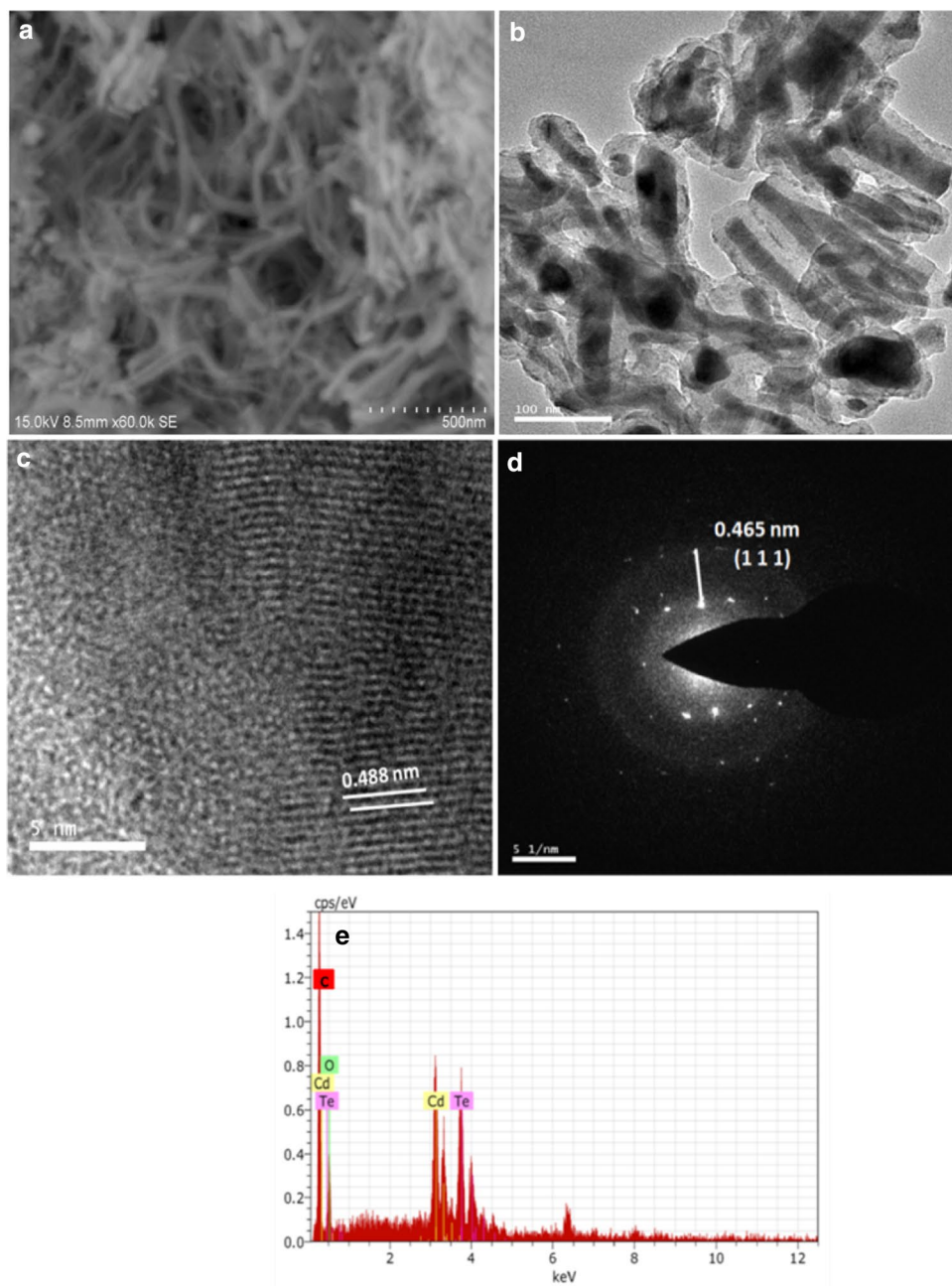


**Fig. 4** **a** Nitrogen adsorption–desorption isotherm and **b** pore size distribution of CdTe NRs

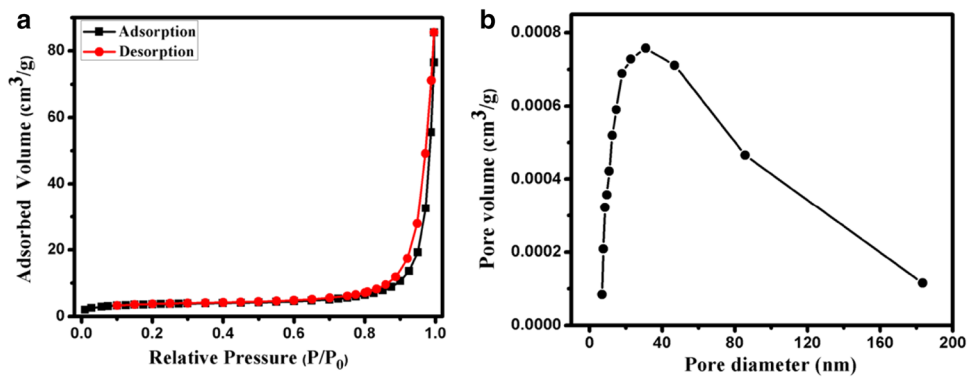
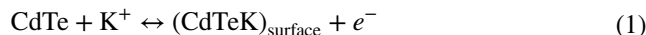


(Fig. 4b). The CdTe NRs raise the electron transfer and mass transport as electrodes in the electrochemical process. This could enhance the electrochemical properties.

### 3.3 Energy storage performance

CdTe NRs display an excellent supercapacitor property with a high specific capacitance and a long cycle life. At first, CV curve of the CdTe electrode has been determined to understand their electrochemical charge storage mechanism. Figure 5a exhibits the CV profile of CdTe electrode for different scan rates of 5, 10, 25, 50 and 100 mV/s and the charge storage mechanism is confirmed by the presence of quasi rectangular curves due to the presence of electrochemical double layers [25]. The specific capacitances for different scan rates are presented in Fig. 5b. The specific capacitance decreases (106, 73, 48, 37 and 27 F/g) with increasing scan rate (5, 10,

25, 50 and 100 mV/s). At lower scan rate, the  $\text{OH}^-$  ions get enough time to diffuse into the inner and outer surfaces of the electrode. But at higher scan rate, intercalation with only the outer surface reduces the capacitance. The redox reaction occurred at the interface of electrode and electrolyte causing intercalation (reduction) and de-intercalation (oxidation) of  $\text{K}^+$  ions is described as [15].



To evaluate the electrochemical properties of CdTe electrode, galvanostatic charging and discharging of the electrode were taken in 2 M KOH electrolyte. The charge–discharge (CD) curves for CdTe electrode for different current densities (2–30  $\text{mA}/\text{cm}^2$ ) are given in

**Fig. 5** **a** CV for different scan rates, **b** variation of specific capacitance with scan rate, **c** charge/discharge curves for different current densities, **d** variation of specific capacitance with current densities, **e** coulombic efficiency and cyclic stability of CdTe NRs at 30  $\text{mA}/\text{cm}^2$  and **f** Ragone plot of CdTe NRs

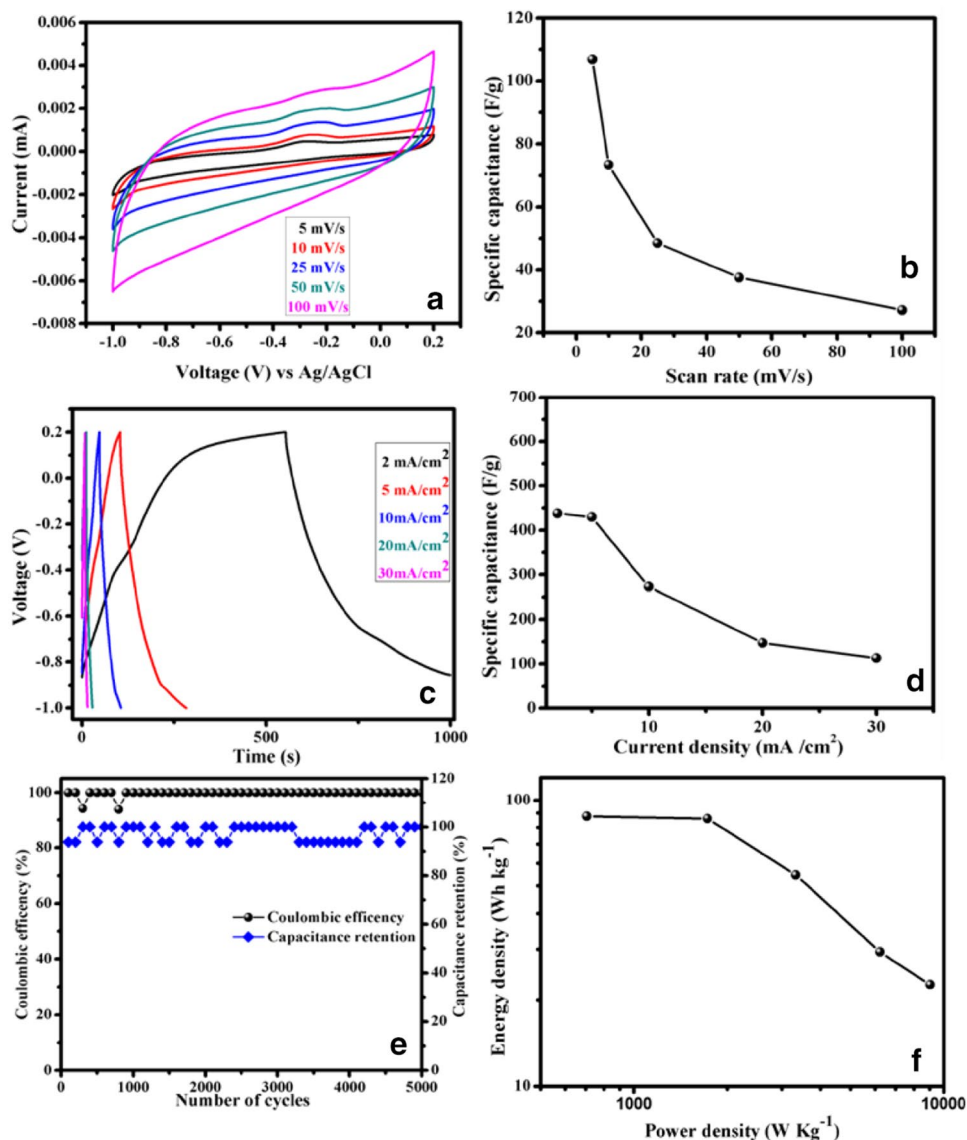


Fig. 5c. The quasi triangular shaped symmetric curves suggest the combined EDLC and pseudocapacitor behavior. The specific capacitance of CdTe electrode is calculated from the discharge curves using the equation [26].

$$C_{sp} = \frac{I\Delta t}{m\Delta V} (F/g) \quad (3)$$

where  $I$  (A) is the charging current,  $\Delta t$  (s) is the discharging time,  $m$  (g) is the mass of active material and  $\Delta V$  (V) is the potential window. Figure 5d shows the specific capacitance of CdTe electrode at different current densities. As in the CD studies, the calculated  $C_{sp}$  is 438, 430, 273, 147 and 113 F/g at current density of 2, 5, 10, 20 and 30 mA/cm<sup>2</sup> respectively. During the fast scan (at higher current density), 29% initial capacitance is retained and may be attributed to only the outer active surface is utilized for charge storage instead of the inner surface. Because at high current density, the electrolyte ions are unable to diffuse into the inner surface of the electrode materials. The long term stability of the electrode was measured by continuous charge–discharge cycles at 30 mA/cm<sup>2</sup> wherein 95% of the capacitance retention has been obtained after 5000 cycles. The Columbic efficiency ( $\eta$ ) was estimated from the equation,

$$\eta = \frac{t_d}{t_c} \times 100\% \quad (4)$$

where  $t_d$  and  $t_c$  are the discharging and charging time with the same current.  $\eta$  is calculated for every 100 cycles up to 5000 cycles which shows the stability  $\sim 99.7\%$  confirming the electrochemical stability of the CdTe electrode as shown in Fig. 5e. This result suggests that CdTe is a suitable electrode material for supercapacitor applications and the values are comparable with the existing reports (Table 1).

Biomolecule assisted CoS nanowires possess high specific capacitance of 508 F/g at a current density of 20 mA/cm<sup>2</sup> with an cyclic stability of 81.2% [6]. Patil et al. have reported the cinnamon like La<sub>2</sub>Te<sub>3</sub> thin film electrode with a high capacitance and current density of 455 F/g and 1 mA/cm<sup>2</sup> respectively. It also shows a good energy and power densities [15]. Electrochemical measurements of flower like CoS<sub>1.097</sub> reveal the superior pseudocapacitor

performance with a high specific capacitance of 555 F/g at 5 mA/cm<sup>2</sup> and excellent cycle life of 98% [27]. Figure 4f shows the Ragone plot for CdTe NRs electrode. The specific energy density and power density are calculated using the equations

$$E = \frac{1}{2} CV^2 \quad (5)$$

$$P = \frac{E}{t} \quad (6)$$

where  $E$  is the energy density (Wh/kg),  $C$  is the specific capacitance (F/g),  $V$  is the potential range (V),  $P$  is the power density (W/kg) and  $t$  is the discharging time (s). CdTe NRs electrode exhibits the high energy density of (87.6 Wh/kg) and power density of (9040 W/kg). This electrode is better energy efficient at high rates.

Figure 6a shows the Nyquist plot in the frequency range from 0.01 to 100 kHz with amplitude of 5 mV and a bias potential of 0.9 V. The impedance spectrum exhibits a semi-circle component at high frequency and linear component at low frequency demonstrating the long term electrochemical stability of the prepared electrode [29]. The resistance of the electrolyte  $R_s$  (0.01  $\Omega$ ) is due to the combination of ionic, electronic and intrinsic of the active electrode. The charge transfer resistance  $R_{ct}$  (1.827  $\Omega$ ) is related to the electroactive surface of the electrode. In the low frequency region, the inclined line is considered as the Warburg impedance which is a constant (0.3). For La<sub>2</sub>Te<sub>3</sub>, in the frequency range of 0.1 Hz to 1 MHz,  $R_s$ ,  $R_{ct}$ , and  $W$  are evaluated as 0.9  $\Omega$ , 0.3  $\Omega$  and 0.04 respectively [15]. The frequency dependent specific capacitance is given by:

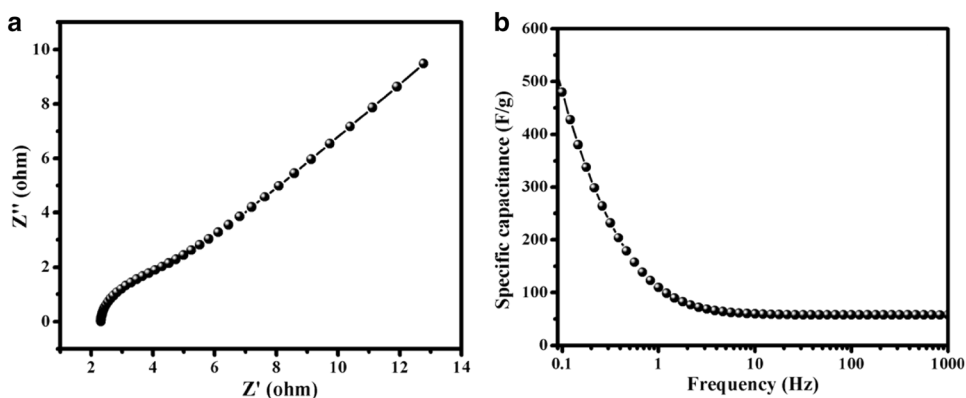
$$C_{sp} = \frac{1}{2\pi f Z''} \quad (7)$$

where  $Z''$  is the impedance. The frequency dependence of specific capacitance is given in Fig. 6b and  $C_{sp}$  at 0.01 Hz is found to be 480 F/g. The specific capacitance increases with decreasing frequency. At the higher frequency side, the electrolytes are hard to diffuse on the surface of the electrode due to the higher resistivity. However, at lower frequency range, the electrode material has a higher capacitive

**Table 1** Comparisons of specific capacitance and cyclic stability for other metal chalcogenides

Electrode	KOH (mole)	Specific capacitance (F/g)/current density (mA/cm <sup>2</sup> )	Stability (%)	References
CoS	3	377/20	74.2	[6]
Te	2	100/30	88	[14]
La <sub>2</sub> Te <sub>3</sub>	1	455/1	71	[15]
CoS <sub>1.097</sub>	2	555/5	98.6	[27]
NiSe <sub>2</sub>	1	75/1	94	[28]
CdTe	2	113/30	99.7	Present work

**Fig. 6** **a** Impedance plot and **b** Frequency dependent specific capacitance of CdTe NRs



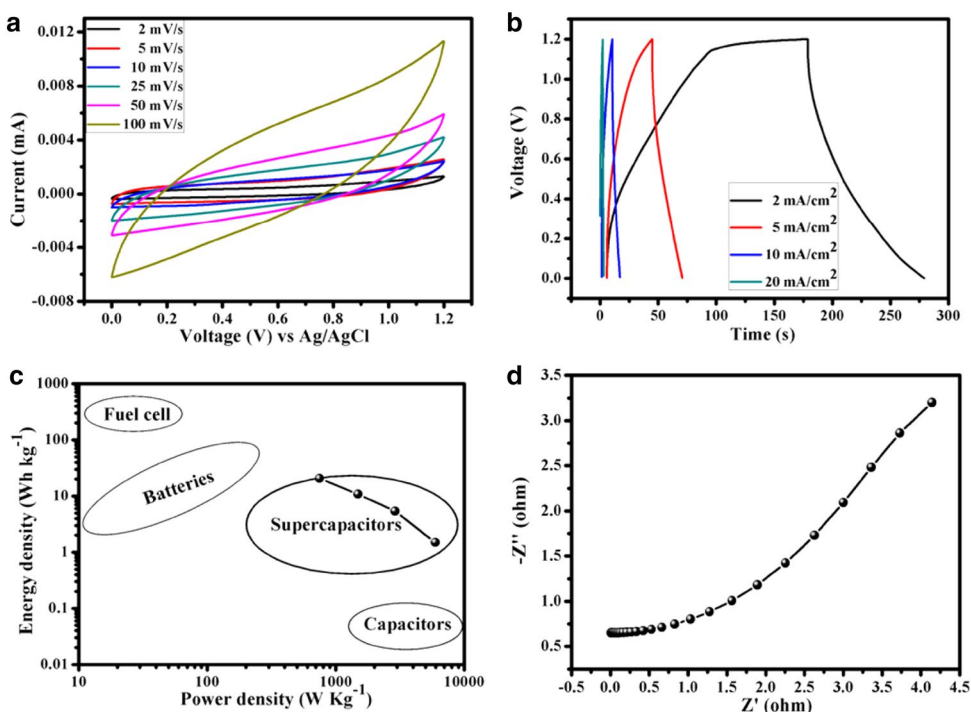
behavior which can access more number of electrolyte ions on the surface results the enhancement of the supercapacitor behavior [30].

### 3.4 Symmetric supercapacitor

The CV curve collected at different current scan rate from 2 to 100 mV/s for CdTe symmetric supercapacitor is shown in Fig. 7a. CV curve posses near rectangular shape due to the presence of EDLC. The calculated specific capacitance of symmetric supercapacitor is decreases (104, 84, 44, 30, 22 and 17 F/g) with the scan rate (2, 5, 10, 25, 50 and 100 mV/s). The GCD curve with various current densities with voltage window of 0–1.2 V are shown in Fig. 7b. The calculated specific capacitance of CdTe symmetric device is 103, 54, 27 and 7 F/g at current

densities of 2.5, 5, 10 and 20 mA/cm<sup>2</sup> respectively. Moreover, the symmetric supercapacitor based on CdTe delivers the energy density ranges from 20.54 to 1.49 Wh/kg, the power density ranges from 746 to 5960 W/kg (Fig. 7c), which indicates that the CdTe based supercapacitor is a potential candidate for electronic applications. Figure 7d shows EIS in the frequency range from 0.01 to 100 kHz at open-circuit potential with an AC perturbation of 5 mV used to analyze the internal resistance of the device. EIS exhibits a semicircle component at a high frequency and a linear component at low frequency indicates the long term electrochemical stability of the CdTe electrode. Semicircle in the higher frequency region belongs to the charge transfer resistance and in the low frequency reveals the Warburg impedance of the electrode.

**Fig. 7** Symmetric device of CdTe NRs **a** CV for different scan rates, **b** charge/discharge curve for different current densities, **c** Ragone plot of symmetric device and **d** EIS profile



## 4 Conclusion

CdTe NRs were successfully synthesized through hydrothermal process using ascorbic acid as a reducing agent. Notably, the synthesized CdTe NRs offer a remarkable performance over the reported supercapacitors. CdTe electrode shows a good electrochemical performance with a specific capacitance of 438 F/g at a current density of 2 mA/cm<sup>2</sup>. Capacitance retention of 95% is retained even after 5000 cycles at the current density of 30 mA/cm<sup>2</sup>. The maximum specific capacitance of CdTe electrode in symmetric supercapacitor is 103 F/g at current density of 2.5 mA/cm<sup>2</sup> and this device delivers the high energy density of (20.54 Wh/kg) and power density of (746 W/kg). The above findings may open up a new route for the practical applications of CdTe NRs electrodes in the next generation supercapacitor devices.

**Acknowledgements** The authors would like to thank Prof. S. Ramaprabhu, Indian Institute of Technology Madras, Chennai for BET analysis.

## Compliance with ethical standards

**Conflict of interest** The authors declare no competing financial interest.

## References

- L. Jiang, Y.J. Zhu, *Eur. J. Inorg. Chem.* **8**, 1238–1243 (2010)
- A.G. Shiravizadeh, S.M. Elahi, S.A. Sebt, R. Yousefi, *J. Appl. Phys.* **123**, 083102 (2018)
- R. Yousefi, H.R. Azimi, M.R. Mahmoudian, W.J. Basirun, *Appl. Surf. Sci.* **435**, 886–893 (2018)
- M.A. Baghchesara, M. Cheraghizade, F.J. Sheini, R. Yousefi, *J. Mater. Sci.: Mater. Electron.* **28**, 4475–4480 (2017)
- A.G. Shiravizadeh, R. Yousefi, S.M. Elahi, S.A. Sebt, *Phys. Chem. Chem. Phys.* **19**, 18089–18098 (2017)
- S.J. Bao, C.M. Li, C.X. Guo, Y. Qiao, *J. Power Sources* **180**, 676–681 (2008)
- Y. Li, H. Xie, J. Tu, *Mater. Lett.* **63**, 1785–1787 (2009)
- V.S. Kumbhar, A.C. Lokhande, N.S. Gaikwad, C.D. Lokhande, *Chem. Phys. Lett.* **645**, 112–117 (2016)
- V.S. Kumbhar, A.D. Jagdale, C.D. Lokhande, *J. Power Sources* **234**, 107–110 (2013)
- S.K. Balasingam, M. Lee, B.H. Kim, J.S. Lee, Y. Jun, *Dalton Trans.* **46**, 2122–2128 (2017)
- B. Balamuralitharan, S.N. Karthick, S.K. Balasingam, K.V. Hemalatha, S. Selvam, J. Anandharaj, K. Prabakar, Y. Jun, H.-J. Kim, *Energy Technol.* **5**, 1953–1962 (2017)
- C. Han, Z. Li, W. Li, S. Chou, S. Dou, *J. Mater. Chem. A* **2**, 11683–11690 (2014)
- C. Wei, C. Cheng, Y. Cheng, Y. Wang, Y. Xu, W. Du, H. Pang, *Dalton Trans.* **44**, 17278–17285 (2015)
- M. Manikandan, S. Dhanuskodi, N. Maheswari, C. Muralidharan, C. Revathi, R.T. Rajendra Kumar, G. Mohan Rao, *Sens. Biosens. Res.* **13**, 40–48 (2017)
- S.J. Patil, B.H. Patil, R.N. Bulakhe, C.D. Lokhande, *RSC Adv.* **4**, 56332–56341 (2014)
- M.C. Kum, B.Y. Yoo, Y.W. Rheem, K.N. Bozhilov, W. Chen, A. Mulchandani, N.V. Myung, *Nanotechnology* **8**, 325711 (2008)
- Y. Ye, L. Dia, T. Sun, L.P. You, R. Zhu, J.Y. Gao, R.M. Peng, D.P. Yu, G.G. Qin, *J. Appl. Phys.* **108**, 044301 (2010)
- C.M. Ruiz, E. Saucedo, O. Martinez, V. Bermudez, *J. Phys. Chem. C* **111**, 5588–5591 (2007)
- B. Maniscalco, A. Abbas, J.W. Bowers, P.M. Kaminski, K. Bass, G. West, J.M. Walls, *Thin Solid Film* **582**, 115–119 (2015)
- M.H. Akhlaghi, M.R. Mohammadi, *J. Mater. Sci.* **24**, 3564–3574 (2013)
- X. Xie, S.Y. Kwok, Z. Lu, Y. Liu, Y. Cao, L. Luo, J.A. Zapien, I. Bello, C.S. Lee, S.T. Lee, W. Zhang, *Nanoscale* **4**, 2914–2919 (2014)
- S.F. Tie, C.W. Tan, *Renew. Sustain. Energy Rev.* **20**, 82–102 (2013)
- F. Putois, *J. Power Sources* **57**, 67–70 (1995)
- S.M. Yong, P. Muralidharan, S.H. Jo, D.K. Kim, *Mater. Lett.* **64**, 1551–1554 (2010)
- K. Krishnamoorthy, G.K. Veerasubramani, P. Pazhamalai, S.J. Kim, *Electrochim. Acta* **190**, 305–312 (2016)
- S. Vijayakumar, A.K. Ponnalagi, S. Nagamathu, G. Muralidharan, *Electrochim. Acta* **106**, 500–505 (2013)
- Q. Wang, L. Jiao, H. Du, J. Yang, Q. Huan, W. Peng, Y. Si, Y. Wang, H. Yuan, *Cryst. Eng. Commun.* **13**, 6960–6963 (2011)
- N.S. Arul, J.I. Han, *Mater. Lett.* **181**, 345–349 (2016)
- Y. Lu, K. Qiu, D. Zhang, J. Lin, J. Xu, X. Liu, C. Tang, J.K. Kim, Y. Luo, *RSC Adv.* **4**, 46814–46822 (2014)
- S. Vijayakumar, G. Muralidharan, *J. Electroanal. Chem.* **727**, 53–58 (2014)